PAPER

Dual fluorescent phenanthridinones and crinasiadine derivatives by consecutive palladium-catalyzed three-component syntheses

Regina Kohlbecher and Thomas J. J. Müller ⓘ *

The sequential concatenation of Buchwald–Hartwig amination, Suzuki coupling, and lactamization in a consecutive palladium-catalyzed three-component synthesis provides direct access to functionalized *N*-arylsubstituted phenanthridinones and alkaloid-analogous crinasiadines starting from simple, readily available *ortho*-bromoanilines. A modified reaction sequence, consisting of Suzuki coupling, amide bond formation (lactamization), and subsequent alkylation at the amide nitrogen, provides *N*-alkylsubstituted phenanthridinones and crinasiadines, including two natural products, which are known for their cytotoxic activity against various cancer cell lines. A comprehensive investigation of the photophysical properties reveals dual emission of the *N*-aryl substituted derivatives, characterized by locally excited states (LE band) and intramolecular charge transfer states (CT band). Quantum chemical calculations rationalize the dual emission and suggest that the LE band derives from the *pseudo-N-intra* conformation, whereas the CT band arises from the *pseudo-N-extra* conformation in the excited state.

Introduction

Phenanthridinones are major heterocyclic building blocks that occur in a variety of complex natural products and pharmaceuticals, exhibiting a broad spectrum of pharmacological activities.[1,2] The significance of their scaffolds has aroused great interest in synthetic and medicinal chemistry to design new methodologies and novel derivatives of pharmaceutical relevance.[3]

The access to phenanthridinones is facilitated through a wide range of methods, encompassing both traditional and innovative strategies.[3] Gräbe and Wander first synthesized 6(5*H*)-phenanthridinone in 1893, starting from 2′-aminobiphenyl-2-carboxylic acid.[4] Later, numerous additional methods, such as the alkaline hydroxylation of phenanthridine,[5] Beckmann rearrangement,[6] or anomalous Schmidt reaction,[7] were reported. However, these classical methods have limitations as they often require multistep syntheses of the starting materials and generally result in low to moderate overall yields. Therefore, the quest for methods using environmentally benign chemicals, energy efficient microwave-assisted reactions, and catalytic processes has become increasingly interesting.[3] In 2013, Tanimoto *et al.* established an efficient one-step synthesis of *N*-unsubstituted phenanthridinones, including the natural product phenaglydon.[8] This method implements 2-halobenzoates and 2-aminophenylboronic acids

in a Pd-catalyzed Suzuki coupling reaction.[3,8] The phenanthridinone scaffold is a frequently occurring structural motif in bioactive plant alkaloids.[3,9] For instance, the phenanthridinone-based alkaloid oxynitidine was isolated from the methanol extracts of the root bark and wood of the climbing plant *Zanthoxylum nitidum* (Fig. 1, left).[10–12] These dried plant extracts are known for their anti-inflammatory, analgesic, antimicrobial, and anticancer properties in traditional Chinese medicine.[11,13] The scaffold is also found in various Amaryllidaceae alkaloids, which exhibit antiproliferative effects on cancer cells.[14–18] For instance, three crinasiadines (Fig. 1) were isolated from the Amaryllidaceae plant *Zephyranthes candida*, where *N*-phenethylcrinasiadine exhibits the strongest cytotoxicity against leukemia, lung, and colon cancer cell lines.[19]

Recent research highlights the broad pharmacological potential of phenanthridinones, including anticancer activity,[20] PARP1 inhibition,[21,22] cardioprotective effects,[23,24] regulation of cholesterol metabolism,[25–28] topoisomerase I inhibition,[3,29] and estrogen receptor modulation.[30]

Phenanthridinone derivatives are also gaining increasing interest in the field of organic electronics.[31–33] In particular, the
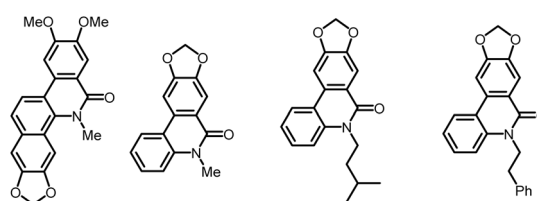
Heinrich Heine University Duesseldorf, Faculty of Mathematics and Natural Sciences, Institute of Organic Chemistry and Macromolecular Chemistry, Universitätstrasse 1, Düsseldorf D-40225, Germany. E-mail: ThomasJJ.Mueller@hhu.de

Fig. 1 Phenanthridinone-based natural products.

photophysical properties of novel phenanthridinones have only scarcely been recognized so far, as they can provide valuable information on SAR, especially since some are known for their dual emission behavior.[34,35]

Multicomponent reactions (MCRs) of functional chromophores enable rapid and diversity-oriented syntheses of compound libraries.[36–38] By definition, MCRs allow for the synthesis of target structures from three or more reactants in a single reaction vessel, ensuring that significant parts of the employed starting materials are incorporated into the final product while drastically reducing the operational effort required for isolation.[36–41]

Recently, the concatenation of Suzuki coupling and Buchwald–Hartwig amination in a consecutive sequentially palladium-catalyzed MCR has successfully paved avenues to libraries of functionalized phenothiazines, carbazoles, indoles, and triarylamines.[42] Herein, we report a novel, diversified, and sequentially palladium-catalyzed MCR that allows direct access to functionalized phenanthridinones as well as alkaloid-analogous crinasiadines starting from simple, readily available starting materials. Additionally, investigations of the photophysical properties and quantum chemical calculations open up a deeper understanding of the electronic structure of phenanthridinone derivatives.

Results and discussion

Syntheses

Starting from *ortho*-bromoaniline **1**, a palladium-catalyzed three-component synthesis was envisioned to provide direct access to phenanthridinones and crinasiadines. After comprehensive optimization (for details see SI, chpt. 5.1), a novel Buchwald-Hartwig amination-Suzuki coupling-lactamization sequence (BHSL-sequence) was developed, based on a previously optimized, highly diversified, sequentially palladium-catalyzed one-pot process for the synthesis of *para*-biaryl-substituted triarylamines (*p*-bTAA).[43] This approach aims to construct a substance library of diverse phenanthridinone derivatives in a modular manner. By switching the Buchwald-Hartwig amination and the Suzuki coupling compared to the *p*-bTAA synthesis,[43] the formation of poorly soluble 6(5*H*)-phenanthridinone intermediates could be circumvented, enabling the successful synthesis of the target molecules. Due to their reactivity, the first step of the Buchwald–Hartwig amination requires an aryl iodide **2** and an *ortho*-bromoaniline **1** to exclude homocoupling of the aniline.[44] Additionally, the aryl iodide should only be employed in one equivalent to avoid twofold arylation of the aniline nitrogen. Furthermore, anhydrous conditions have to be ensured in this step, as traces of water might convert NaO*t*Bu into sodium hydroxide, thereby reducing reaction efficiency due to its lower basicity.[45] In the next step, cyclization between the aniline intermediate and a 2-(ethoxycarbonyl)arylboronic acid **3** has to be initiated. In addition to the Suzuki coupling, the *N*-arylaniline as a nucleophile should attack the ethyl ester to form the lactam. The addition of water and Cs₂CO₃ in this step suppresses the formation of the undesired dihydrophenazine byproduct (see SI). Ultimately,
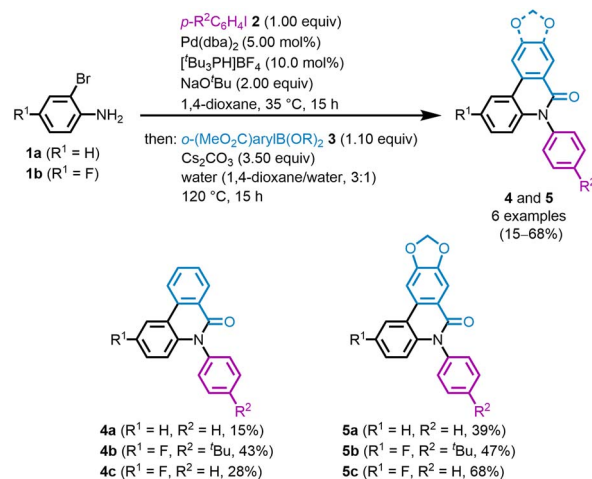
Scheme 1 BHSL synthesis of *N*-arylphenanthridinones **4** and *N*-aryl-crinasiadines **5** (all reactions were performed on a 0.5 mmol scale in 1,4-dioxane (3.5 mL) and yields are given after purification by flash chromatography on silica gel).

ortho-bromoanilines **1** and aryl iodides **2** are successfully subjected to Buchwald–Hartwig amination in the presence of catalytic amounts of Pd(dba)₂ and [*t*Bu₃PH]BF₄, as well as an excess of NaO*t*Bu, at 35 °C for 15 h. The subsequent addition of 2-(methoxycarbonyl)arylboronic acids **3**, Cs₂CO₃, and water at 120 °C for 15 h induces cyclization, affording after flash chromatography three *N*-arylphenanthridinones **4** and three *N*-arylcrinasiadines **5** in moderate to good yields ranging from 15 to 68% (Scheme 1). This corresponds to a yield per bond formation of up to 89%. The presence of a fluoro substituent and a *tert*-butyl group improves solubility and consequently leads to higher yields. The benzodioxole boronic acid ester **3b** required for the preparation of *N*-arylcrinasiadines **5** can be successfully synthesized from piperonal according to a literature protocol (see SI).[46–48] In comparison to *N*-arylphenanthridinones **4**, the 1,3-benzodioxole causes an increase in yield, possibly due to improved solubility and easier purification of *N*-arylcrinasiadines **5**.

Furthermore, the optimized Suzuki coupling can be successfully combined with lactamization and nucleophilic substitution in a consecutive three-component reaction (see SI). Here, a solvent mixture of 1,4-dioxane and DMF in a ratio of 2 : 1 is used for the Suzuki coupling, which increases the solubility of the 6(5*H*)-phenanthridinone intermediate and allows the subsequent alkylation of the lactam nitrogen with alkyl halides **2** to proceed more efficiently. In addition, an iodoaniline **1** is used in the first step, as iodides are more reactive than bromides.[44] The Suzuki coupling-lactamization-substitution (SLS) sequence finally provides after flash chromatography, access to three *N*-alkylphenanthridinones **6** and two *N*-alkylcrinasiadines **7** with yields ranging from 7 to 44% (Scheme 2). These include the two natural products *N*-methylcrinasiadin **7a** and *N*-phenethylcrinasiadin **7b**, which are known for their cytotoxicity against leukemia, lung, and colon cancer cells.[19] The literature known syntheses to date for the preparation of **7a** and **7b** are multi-step syntheses, but no one-pot methodologies,
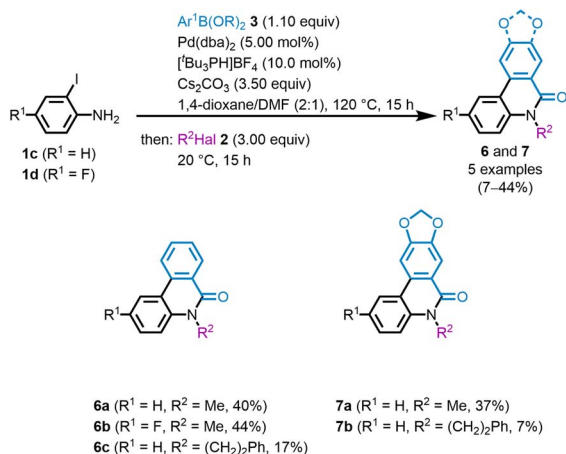
Scheme 2 SLS sequence of *N*-alkylphenanthridinones **6** and *N*-alkylcrinasiadines **7** (all reactions were performed on a 0.5 mmol scale in 1,4-dioxane (3.5 mL) and yields are given after purification by flash chromatography on silica gel).
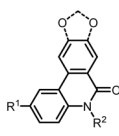
i.e., consecutive MCR.[19,49] The incorporation of a fluorine substituent in derivative **6b** improves solubility and consequently leads to the highest yield. In addition to methyl iodide (**2c**), (2-bromoethyl)benzene (**2d**) can also be employed in the terminal alkylation. However, the inclusion of **2d** leads to a lower yield. It cannot be excluded that the presence of the palladium catalyst triggers the dehydrobromination of the substrate by competing β-H-elimination.[50]

The structures of all phenanthridinone analogues **4–7** were assigned by extensive NMR spectroscopy, mass spectrometry, and IR spectroscopy (see SI). In addition, the molecular composition of the novel compounds was determined by HPLC-HRMS (see SI).

Photophysical properties

Although *N*-arylphenanthridinones have been shown to display dual emission,[34,35] the ease of their accessibility through our one-pot sequence prompted us to take a closer look at the photophysics, in particular, to scrutinize the origin of the

Table 1 Selected photophysical properties (absorption maxima in solution with absorption coefficients ε and emission maxima in solution with fluorescence quantum yields Φ_{em} and Stokes shifts $\Delta\tilde{\nu}_s$) of all phenanthridinones **4–7**

Compound	R^1	R^2	Solvent	$\lambda_{max,abs}{}^a$ [nm] (ε [M^{-1} cm^{-1}])	$\lambda_{max,em}{}^b$ [nm]/$\Delta\tilde{\nu}_s{}^d$ [cm^{-1}] (Φ_{em})^c
4a	H	Ph	CH$_2$Cl$_2$	232 (35 300), 237 (35 000), 260 (13 200), 306 (7200), 322 (7300), 336 (5700)	372/2900, 524/10 700
4b	F	*p*-^{t}BuC$_6$H$_4$	CH$_2$Cl$_2$	237 (34 700), 261 (13 000), 273 (sh, 8100), 319 (5400), 331 (7200), 345 (sh, 6100)	382/2800, 530/10 100 (0.01)
			MeCN	243 (sh, 40 700), 248 (44 100), 255 (sh, 41 900), 281 (sh, 14 100), 291 (sh, 9400), 329 (sh, 8300), 348 (8400), 363 (sh, 7100)	376/2600, 579/10 300
4c	F	Ph	CH$_2$Cl$_2$	236 (41 000), 260 (15 100), 272 (sh, 9600), 314 (6100), 329 (8900), 343 (7400)	374/2400, 548/10 900
5a	H	Ph	CH$_2$Cl$_2$	249 (4800), 270 (15 700), 286 (sh, 10 900), 296 (sh, 9700), 311 (sh, 11 500), 318 (11 500), 339 (6600)	367/2100, 519/12 200
5b	F	*p*-^{t}BuC$_6$H$_4$	CH$_2$Cl$_2$	249 (43 400), 274 (13 100), 287 (sh, 10 500), 298 (sh, 8200), 317 (sh, 9700), 329 (10 300), 346 (8000)	372/2000, 550/10 700 (0.02)
			MeCN	247 (35 600), 268 (35 500), 292 (sh, 10 200), 306 (sh, 8100), 316 (sh, 6700), 328 (sh, 8400), 345 (6400), 365 (6300)	372/2100, 562/9600
5c	F	Ph	CH$_2$Cl$_2$	248 (16 900), 273 (5200), 287 (4200), 299 (3400), 316 (sh, 3800), 329 (3900), 346 (5300)	371/2000, 543/10 500
6a	H	Me	CH$_2$Cl$_2$	233 (49 200), 239 (50 000), 262 (18 600), 276 (sh, 9000), 312 (sh, 7000), 325 (9700), 339 (7600)	367/2300
6b	F	Me	CH$_2$Cl$_2$	236 (39 500), 253 (13 100), 262 (15 700), 273 (8900), 317 (sh, 6300), 331 (9100), 346 (7700)	373/2100
6c	H	Phenethyl	CH$_2$Cl$_2$	234 (33 400), 240 (34 400), 252 (sh, 12 300), 262 (13 200), 275 (sh, 7100), 310 (sh, 5700), 325 (6400), 339 (5300)	367/2300
7a	H	Me	CH$_2$Cl$_2$	247 (45 000), 269 (17 300), 285 (sh, 10 500), 297 (sh, 9500), 313 (sh, 12 800), 319 (11 900), 324 (sh, 11 100), 340 (8700)	364/2000
7b	H	Phenethyl	CH$_2$Cl$_2$	249 (35 700), 270 (15 900), 286 (sh, 8400), 297 (sh, 7500), 313 (sh, 8700), 318 (8700), 325 (sh, 8100), 340 (5400)	364/2000

^{a} Recorded at $T = 293$ K, $c = 10^{-5}$ M. ^{b} Recorded at $T = 293$ K, $c = 10^{-7}$ M. ^{c} Absolute over all quantum yields recorded at $T = 293$ K, $c = 10^{-6}$ M. ^{d} $\Delta\tilde{\nu}_s = 1/\lambda_{max,abs} - 1/\lambda_{max,em}$.

observed dual emission. This phenomenon was attributed to a conformational change of the N-aryl substituent as supported by solvatochromism and time-resolved fluorescence studies.[35] Alternatively, an anti-Kasha behavior was discussed, which involves emission from higher excited states as substantiated by quantum chemical calculations.[34] Therefore, the photophysical properties of all compounds were investigated by UV/vis absorption and fluorescence spectroscopy in dichloromethane or acetonitrile (Table 1).

The N-aryl/N-alkylphenanthridinones **4** and **6** exhibit an intense absorption maximum with a shoulder at high energy in the UV. In contrast, the N-aryl/N-alkylcrinasiadines **5** and **7** display only one characteristic maximum without a shoulder in this region, which, unlike compounds **4** and **6**, is slightly bathochromically shifted. The subsequent longer wavelength maxima of compounds **5** and **7** are also slightly bathochromically shifted in comparison to **4** and **6**. At lowest energy, three maxima appear for each compound, which are attributed to vibronic fine structure of the same electronic transition. The longest wavelength absorption maxima of all compounds **4–7** occurring at a similar wavelength to that of the unsubstituted 6(5H)-phenanthridinone **8** (R=H, isolated intermediate) (Fig. 2). Therefore, the longest wavelength absorption maximum of all compounds probably corresponds to the HOMO → LUMO transition, in accordance with literature for compound **8**.[35,51]

Furthermore, the absorption maxima at lower energy of the N-aryl/N-alkylphenanthridinones **4b–c** and **6b**, as well as the N-arylcrinasiadines **5b–c**, are very similar and slightly bathochromically shifted compared to compounds **4a, 5a, 6a, 6c,** and **7a–b** devoid of fluorine substituent at position R[1]. Consequently, the substituent at position R[2], unlike that at position R[1], has only a minor influence on the spectra for the present derivatives. Therefore, it can be assumed that the longest wavelength absorption band is primarily associated with the phenanthridinone moiety.

The polarity of the solvents influences the position of the absorption maxima, as illustrated by the bathochromic shift observed in acetonitrile (Table 1). This suggests that the absorption bands cannot be attributed solely to a locally excited state (LE band), but rather also possess partial charge transfer (CT) character. The shapes of the absorption bands remain largely unchanged, which indicates a structurally similar electronic transition in both solvents (Fig. 3).

The emission spectra of the N-arylsubstituted compounds **4** and **5** show two emission maxima, in contrast to those of the N-alkylsubstituted compounds **6** and **7**, which indicate dual fluorescence (Fig. 4). The shorter wavelength emission band only displays a small Stokes shift $\Delta\tilde{\nu}_s$, indicating emission from an LE band, as only minor geometric changes are likely to occur between the ground and excited states. Moreover, the shape and position of the LE band closely resemble the emission maximum of 6(5H)-phenanthridinone **8** (Fig. 2).[35,51] The emission is therefore likely to originate from the phenanthridinone core.

The second emission maximum is, unlike the LE band, strongly bathochromically shifted. This maximum is only weakly significant for compounds **4c** and **5c**, which bear a fluorine substituent at R[1] and no substituent at R[2]. Investigations of the emission of **4b** and **5b** in dichloromethane and acetonitrile reveal that the intensity of the longer wavelength emission band increases relative to the LE band with increasing solvent polarity (Fig. 4). Moreover, since in acetonitrile the LE transition hardly shifts, the insensitivity to solvent polarity (Table 1) can be attributed to a π–π* transition. In contrast, the longer wavelength emission maxima exhibit a pronounced bathochromic shift with increasing polarity form dichloromethane to acetonitrile (positive solvatochromism). This emission maximum is therefore likely a CT band, as polar solvents
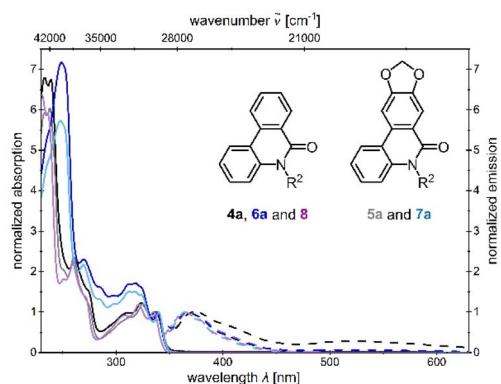

Fig. 2 Comparison of the normalized UV/vis absorption and emission spectra of phenanthridinones **4a, 5a, 6a, 7a** and 6(5H)-phenanthridinone **8** (absorption spectra recorded in CH₂Cl₂, T = 293 K, c = 10⁻⁵ M (bold lines) and emission spectra recorded in CH₂Cl₂, T = 293 K, c = 10⁻⁷ M (dashed lines)).
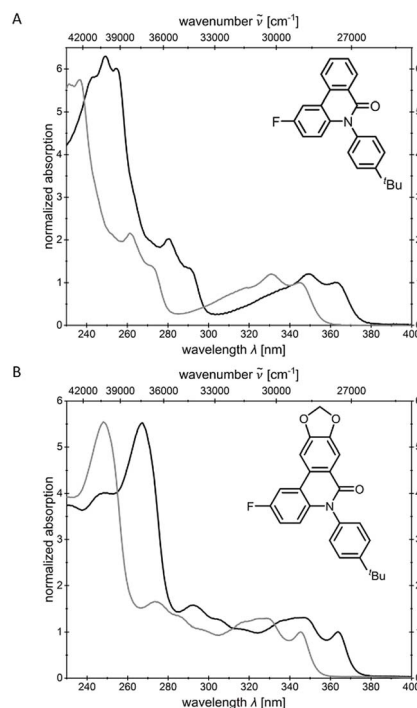

Fig. 3 Comparison of the normalized absorption spectra of N-arylphenanthridinone derivatives **4b** (A) and **5b** (B) in acetonitrile (black lines) and dichloromethane (gray lines) (T = 293 K, c = 10⁻⁵ M).
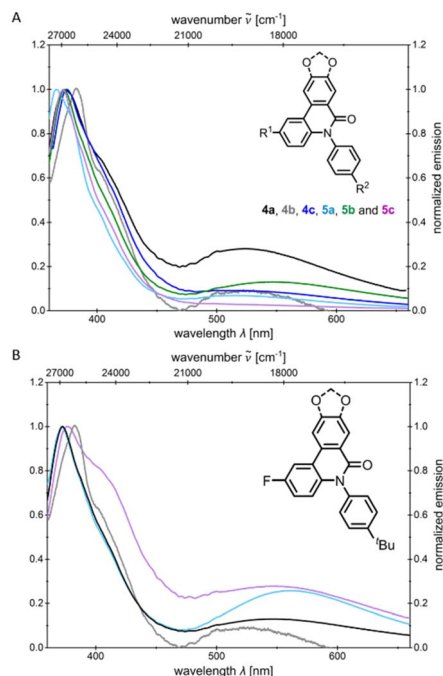
Fig. 4 Normalized emission spectra of *N*-arylphenanthridinone derivatives **4**−**5** in CH$_2$Cl$_2$ (A) and comparison of emission spectra of **4b** and **5b** in CH$_2$Cl$_2$ and of **4b** and **5b** in MeCN (B) (emission spectra recorded in CH$_2$Cl$_2$ or MeCN, $T = 293$ K, $c = 10^{-7}$ M).

stabilize charge separation more effectively than nonpolar ones.[35] However, the LE emission remains more dominant in both solvents. Independent of the excitation wavelength the emission maxima appear at the same wavelength. The degassed and non-degassed emission spectra of compounds **4b** and **5b** in acetonitrile differ only marginally (see SI), which likely rules out the assignment of the longest wavelength emission band to be phosphorescence. Quantum chemical calculations might unravel the origin of the bands, either from a higher excited state (anti-Kasha behavior)[34] or from a conformational change[35] in the first excited state (*vide infra*).

Overall, a comparison of the emission spectra of the *N*-alkyl substituted compounds **6** and **7**, as well as 6(5*H*)-phenanthridinone **8** (see SI), indicates that the presence of an aryl group at the nitrogen is essential for the occurrence of dual emission, as both an LE and a CT band were only observed for compounds **4** and **5**. Furthermore, the nature of the substituents at positions R^1 and R^2 influences the intensity ratio of the LE to the CT band. The CT emission increases relative to the LE band for R^1 bearing an electron-withdrawing substituent and for R^2 bearing an electron-donating substituent, which is consistent with observations of Demeter *et al.*[35] This additionally supports the hypothesis of a population of the phenanthridinone core in the excited state, which might be scrutinized through theoretical analyses (*vide infra*).

The absolute fluorescence quantum yield Φ_{em} could only be determined for compounds **4b** and **5b**, with values of 1% and 2%, respectively, whereas the other compounds exhibit emission that is too weak to be recorded (Table 1). At room temperature, the dominant deactivation process of the excited

S_1 state in phenanthridinones is intersystem crossing (ISC) to the triplet state, which accounts for the very low fluorescence quantum yield Φ_{em}.[35]

Calculated electronic structure

A deeper insight into the electronic structure of *N*-arylphenanthridinones **4** and *N*-arylcrinasiadines **5** can be obtained by (TD)DFT calculations exemplarily for compounds **4b** and **5b** with the program package Gaussian 16.[52] In analogy to the literature, the B3LYP[53,54] functional and the Pople basis set 6-31G* (ref. 55) were employed for the quantum chemical analysis of the phenanthridinones.[34] All minima were confirmed unambiguously by analytical frequency analysis (NIMAG = 0). Based on the absorption and emission properties in solution, the intrinsic polarizable continuum model (PCM) with dichloromethane as the dielectric medium was applied in the quantum chemical calculations.[56] The calculated absorption and emission energies agree quantitatively well with the experimental data in dichloromethane for the selected examples, with only minor over- or underestimation of the energy levels (Table 2).

Since the absorption spectra of structures **4b** and **5b** in dichloromethane display very similar profiles, only the calculated absorption spectrum of **4b** will be discussed in detail (Fig. 5). The vertical bars represent the calculated transitions and illustrate that the longest wavelength absorption band is primarily dominated by the HOMO → LUMO transition (Fig. 5A). In the calculated spectrum, the transitions combine into broad bands at both lower and higher energy. In the experimental spectrum, these appear as weakly pronounced shoulders, indicating the superposition of multiple transitions. Frontier molecular orbitals (FMO) are expectedly involved in the dominant electronic transitions (Fig. 5B). The S$_0$–S$_1$ and S$_0$–S$_{13}$ transitions mainly occur between delocalized π-orbitals of the same conjugated system, indicating an LE character of these states. Only the S$_0$–S$_{12}$ transition, in which the electron density is transferred from the more localized HOMO−4 to the delocalized LUMO, suggests a slight CT character. TDDFT calculations showed that S$_1$ predominantly results from the HOMO → LUMO transition. In contrast, the higher excited states are composed of multiple orbital pairs and can thus be interpreted as mixtures of various electronic transitions. The energies of the FMO of compounds **4b** and **5b** are visualized in dichloromethane (Fig. 6). A comparison of *N*-arylphenanthridinone **4b** with the structurally related crinasiadine **5b** reveals that the additional oxygen atoms in crinasiadine exert electron-donating effects, leading to a slight increase of both the HOMO and LUMO energy levels.[57] Since the HOMO is raised slightly higher in comparison to the LUMO, the energy gap $\Delta E(E_{HOMO} - E_{LUMO})$ of crinasiadine **5b** is slightly smaller than that of compound **4b**.

However, this difference is not reflected in the experimental absorption spectra, as the position of the longest-wavelength absorption band is nearly identical for both compounds. This can be explained by the fact that the experimental band results from the superposition of several electronic transitions and therefore cannot be directly equated with the calculated HOMO

Table 2 (TD)DFT calculations on the UV/vis absorption and emission maxima of N-arylphenanthridinone **4b** and N-arylcrinasiadine **5b** (Gaussian 16, B3LYP/6-31G*, PCM CH_2Cl_2, for details see SI)

Com-pound	R^1	R^2	$\lambda_{max,abs(exp)}^{a}$ [nm] (ε [M^{-1} cm^{-1}])	$\lambda_{max,abs(calc)}$ [nm] (oscillator strength f), most dominant contribution	$\lambda_{max,em(exp)}^{b}$ [nm]	$\lambda_{max,em(calc)}$ [nm] (oscillator strength f), most dominant contribution
4b	F	^{t}Bu	237 (34 700)	229 (0.0247) HOMO-3 → LUMO+1 (70%)	382, 530	405 (0.3277) HOMO → LUMO (95%),
				231 (0.3859) HOMO → LUMO+4 (49%)		579 (0.1270) HOMO → LUMO (99%)
				235 (0.2417) HOMO-4 → LUMO (41%)		
				248 (0.0256) HOMO-3 → LUMO (88%)		
			261 (13 000)	256 (0.1342) HOMO-1 → LUMO+1 (47%)		
				269 (0.0506) HOMO-1 → LUMO (71%)		
			273 (sh, 8100)	292 (0.0311) HOMO → LUMO+1 (90%)		
			319 (5400)	316 (0.2320) HOMO → LUMO (93%)		
			331 (7200)			
			345 (sh, 6100)			
5b	F	^{t}Bu	249 (43 400)	241 (0.1814) HOMO → LUMO+4 (53%)	372, 550	386 (0.3533) HOMO → LUMO (96%),
			274 (13 100)	247 (0.5248) HOMO-3 → LUMO (44%)		563 (0.1417) HOMO → LUMO (99%)
			287 (sh, 10 500)	251 (0.0154) HOMO → LUMO+3 (84%)		
				268 (0.1603) HOMO → LUMO (77%)		
				286 (0.1849) HOMO-1 → LUMO (49%)		
			298 (sh, 8200)	301 (0.0114) HOMO → LUMO+1 (51%)		
			317 (sh, 9700)	319 (0.2547) HOMO → LUMO (89%)		
			329 (10 300)			
			346 (8000)			

^{a} Recorded in CH_2Cl_2, $T = 293$ K, $c = 10^{-5}$ M. ^{b} Recorded in CH_2Cl_2, $T = 293$ K, $c = 10^{-7}$ M.

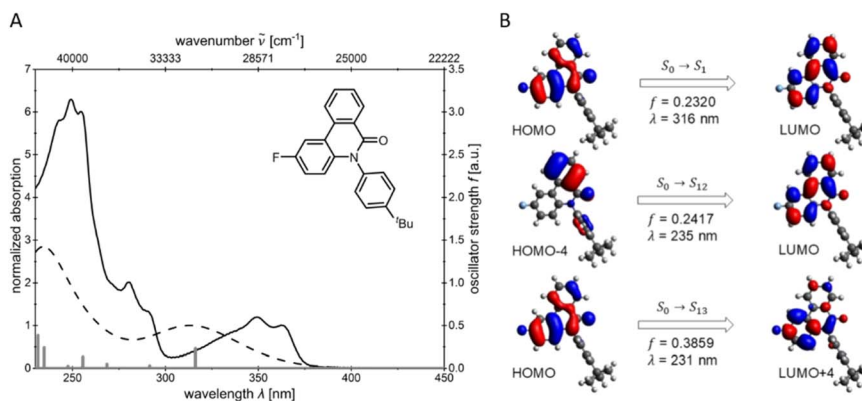Fig. 5 Comparison of the calculated (Gaussian 16, B3LYP/6-31G*, PCM CH_2Cl_2 (dashed lines)) and experimentally determined (recorded in CH_2Cl_2, $T = 293$ K, $c = 10^{-5}$ M (bold lines)) UV/vis spectra of N-arylphenanthridinone **4b** with the calculated transitions shown as gray bars (A) and calculated molecular orbitals of **4b** for the dominant electronic transitions (B) (Gaussian 16, B3LYP/6-31G*, PCM CH_2Cl_2, isosurface value 0.025 a.u.).

→ LUMO transition. For both compounds **4b** and **5b**, the coefficient densities of the HOMO and LUMO are predominantly localized on the phenanthridinone moiety, confirming the LE character of the lowest electronic transitions.

Demeter *et al.* investigated various dual fluorescent N-aryl-phenanthridinones, including N-arylphenanthridinone **4a**. They recorded fluorescence decay curves in both the LE and CT regions of the spectrum and observed biexponential decays. From this, they concluded that the CT state is not directly excited from the ground state but originates instead from the initially excited LE state.[35] They further postulated that the CT state must be significantly more planar than the LE state, as no CT fluorescence is observed in twisted N-arylphenan-thridinones. In these cases, complete planarity is sterically
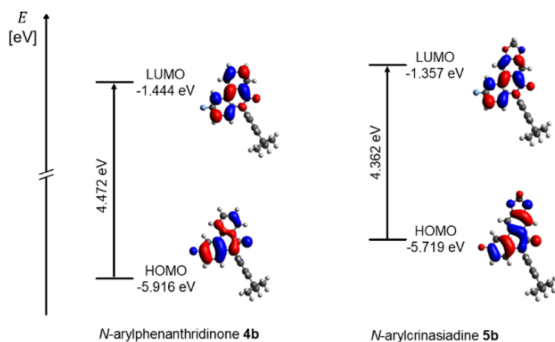
Fig. 6 Selected Kohn–Sham FMO of *N*-arylphenanthridinone **4b** and *N*-arylcrinasiadine **5b** employing the PCM with dichloromethane as solvent (Gaussian 16, B3LYP/6-31G*, PCM CH₂Cl₂, isosurface value at 0.025 a.u.).

hindered by *ortho*-methyl substituents on the aryl group.[35] Based on these results, a potential energy scan was carried out in both the ground (S_0 and S_0^*) and excited states (S_1) to investigate the geometry dependence of the electronic states and possible relaxation pathways between the LE and CT states using quantum chemical methods. The CN-bond rotation was modeled by a torsional scan by 360° rotation of the *N*-aryl substituent with the torsion angle θ (Fig. 7). The initial geometry is defined as a rotational angle θ of 0°. The energy curves of compounds **4b** and **5b** are very analogous in the vibrationally relaxed (S_0) and vibrationally excited (S_0^*) ground states (see SI), with the perpendicular geometry representing the global minimum in each case (NIMAG = 0), *i.e.* thermodynamically preferred conformations. In contrast, the coplanar orientation of the phenanthridinone unit and the aryl substituent occurs in a transition state with an imaginary frequency (NIMAG = 1). This rotational barrier ΔE amounts to 0.72 eV (17.0 kcal mol⁻¹) for compound **4b** and 0.74 eV (17.1 kcal mol⁻¹) for compound **5b**, which can be thermally surmounted at room temperature, yet significantly slowed down kinetically.[58] The rate constants k ($k(\mathbf{4b}) = 4.14$ s⁻¹ and $k(\mathbf{5b}) = 1.90$ s⁻¹) of the rotation around the C–N-bond can be estimated using the Eyring equation[59] to proceed quite slowly.

The energy curves of compounds **4b** and **5b** in the excited state (S_1) also exhibit very similar profiles (see SI). In contrast to the ground states, however, the coplanar geometry (NIMAG = 0) now represents the glo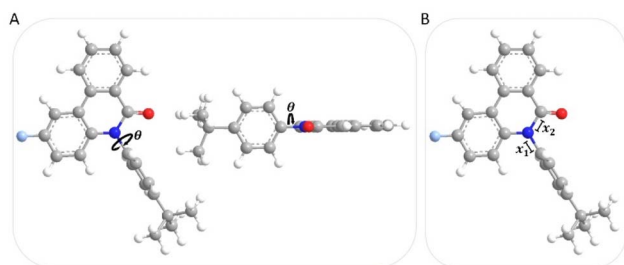bal minimum, while a conformer slightly twisted from a perpendicular geometry constitutes a second local minimum (NIMAG = 0). The coplanar geometry reveals a shorter *N*-aryl bond length x_1, which therefore indicates partial double bond character and suggests a more efficient π-conjugation compared to the perpendicular geometry. Furthermore, the N–CO amide bond length x_2 is elongated in the coplanar geometry. Both geometries resemble the *N-intra* and *N-extra* conformations of phenothiazine.[60] In the *N-intra* conformation, the nitrogen lone pair of phenothiazine overlaps with the π-system of the anellated benzene rings due to the quasi-equatorial orientation of the substituent. In the *N-extra* conformation, the substituent adopts a quasi-axial position. Unlike in phenothiazine, however, the nitrogen atom of the amide group is not sp³-hybridized and pyramidal, but sp²-hybridized and arranged in a trigonal planar geometry.[35,61,62] Therefore, it is more appropriate to refer to a perpendicular *pseudo-N-intra* conformation and a coplanar *pseudo-N-extra* conformation. These two conformations are illustrated exemplarily for compound **4b** (Fig. 8).

The energy barrier $\Delta E(S_1(\text{LE})\text{-}S_1(\text{CT}))$ between the two conformers $S_1(\text{LE})$ and $S_1(\text{CT})$ in the excited state is 0.33 eV (7.61 kcal mol⁻¹) for compound **4b** and 0.30 eV (7.07 kcal mol⁻¹) for compound **5b**, and is easily overcome at room temperature,[58] which may explain the occurrence of dual emission at this temperature. The calculated rate constants k in the excited state ($k(\mathbf{4b}) = 1.63 \times 10^7$ s⁻¹ and $k(\mathbf{5b}) = 5.24 \times 10^7$ s⁻¹) support this hypothesis, as the conformational interconversion proceeds with high efficiency. Assuming a Boltzmann distribution, the theoretical Gibbs free energy ΔG of both conformers ($\Delta G(\mathbf{4b}) = 0.30$ eV (6.89 kcal mol⁻¹) and $\Delta G(\mathbf{5b}) = 0.23$ eV (5.22 kcal mol⁻¹)) yields the equilibrium constants K for dyes **4b** (7.29×10^{-6}) and **5b** (1.27×10^{-4}) corresponding to a population ratio of 99.987 to 0.013 in favor of the coplanar *pseudo-N-extra* conformation $S_1(\text{CT})$. The dual emission is therefore a consequence of the kinetic competition between emission from the *pseudo-N-intra* conformation $S_1(\text{LE})$ and conformational interconversion to conformer $S_1(\text{CT})$, leading to partial emission from both conformers.[35]
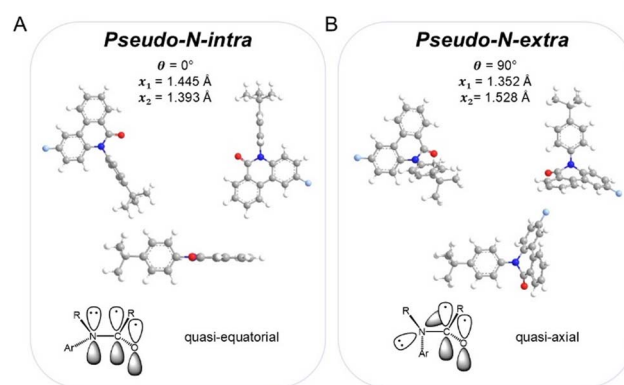

Fig. 8 Comparison of the excited state geometries of *pseudo-N-intra* (A) and *pseudo-N-extra* (B) from different perspectives for compound **4b** (top, Gaussian 16, B3LYP/6-31G*, PCM CH₂Cl₂), along with a schematic representation of the *N*-aryl group (Ar) in the quasi-equatorial *intra*-conformation and quasi-axial *extra*-conformation (bottom, R = anellated benzene rings).

Fig. 7 Illustration of the minimum geometry of **4b** as the starting geometry for the torsion scan with the torsion angle θ, which describes the rotation around the *N*-aryl bond (A), with x_1 as the *N*-aryl bond length and x_2 as the N–CO amide bond length (B).

For a quantitative assessment of the dual emission behavior, the ratio of the integral emission intensities of both bands on a Jacobian energy-corrected scale can be considered (see SI, chpt. 9.5) and compared with the theoretically calculated oscillator strengths.[63] For dye **4b**, the integrated emission spectra give a ratio A_{LE}/A_{CT} of 2.14, while the quantum-chemically calculated oscillator strengths give a ratio f_{LE}/f_{CT} of 2.58. Thus, f_{LE}/f_{CT} moderately overestimates A_{LE}/A_{CT} but remains consistent in trend with the experimental result, thereby supporting the assignment of the two emission channels. For dye **5b**, however, f_{LE}/f_{CT} (= 2.49) does not adequately capture A_{LE}/A_{CT} (= 4.25). The deviations can be attributed to differences in baseline choice and contributions from non-radiative processes.[64,65]

Jabłoński diagrams illustrate the absorption and emission of compounds **4b** (Fig. 9 (A)) and **5b** (Fig. 9(B)). In the *pseudo-N-intra* conformation, the vibrationally excited S_1^* state lies only slightly above the vibrationally relaxed S_1 LE-state in energy (ΔE(**4b**) = 0.32 eV and ΔE(**5b**) = 0.24 eV), which represent small Stokes shifts ($\Delta\tilde{\nu}_{s(exp)}$ (**4b**) = 2800 cm^{-1} *vs.* $\Delta\tilde{\nu}_{s(calc)}$ (**4b**) = 7000 cm^{-1} and $\Delta\tilde{\nu}_{s(exp}$ (**5b**) = 2000 cm^{-1} *vs.* $\Delta\tilde{\nu}_{s(calc)}$ (**5b**) = 5400 cm^{-1}). As a result, only minimal structural changes occur and the aryl substituent only slightly twists. This twisting causes the aryl unit to bear less electron density compared to the Franck–Condon geometry. Nevertheless, the electron density remains predominantly localized on the phenanthridinone moiety. Even after emission from the S_1 state, the coefficient density remains localized on the phenanthridinone core and the resulting transition can be assigned to the short wavelength LE band in the experimental emission spectrum. However, due to coefficient density on the aryl substituent in the vibrationally excited S_0^* state, the transition cannot be regarded as a pure LE transition.

The conformational change to the *pseudo-N-extra* conformer lowers of the excited-state energy level. Planarization enables more efficient delocalization of the electron density, which is also reflected in the shorter *N*-aryl bond length x_1 of the conformer. In the *pseudo-N-extra* conformation, the vibrationally excited S_1^* state lies significantly above the vibrationally relaxed S_1 CT-state in energy (ΔE (**4b**) = 0.58 eV and ΔE (**5b**) = 0.49 eV). As a result of significant structural changes, which cause large Stokes shifts ($\Delta\tilde{\nu}_{s(exp)}$ (**4b**) = 10 100 cm^{-1} *vs.* $\Delta\tilde{\nu}_{s(calc)}$ (**4b**) = 12 800 cm^{-1} and $\Delta\tilde{\nu}_{s(exp)}$ (**5b**) = 10 700 cm^{-1} *vs.* $\Delta\tilde{\nu}_{s(calc)}$ (**5b**) = 13 200 cm^{-1}) and a smaller energy gap ΔE, the redshifted emission is observed. Therefore, S_1–S_0^* CT-transition from the phenanthridinone to the aryl unit occurs. The coefficient distribution of the T_1 state of the *pseudo-N-intra* conformation is for both compounds **4b** and **5b** very similar to the S_1 state but lies energetically well below the S_1 state of the *pseudo-N-extra* conformation (see SI).

Nevertheless, according to El-Sayed's rule ISC of similar transitions can be considered to occur less probable.[66] The quantum chemically calculated phosphorescence of compounds **4b** and **5b** corresponds well with the experimentally observed long-wave emission bands. But the nearly identical experimental emission spectra in degassed and non-degassed solutions (see SI) indicate that no significant oxygen-induced
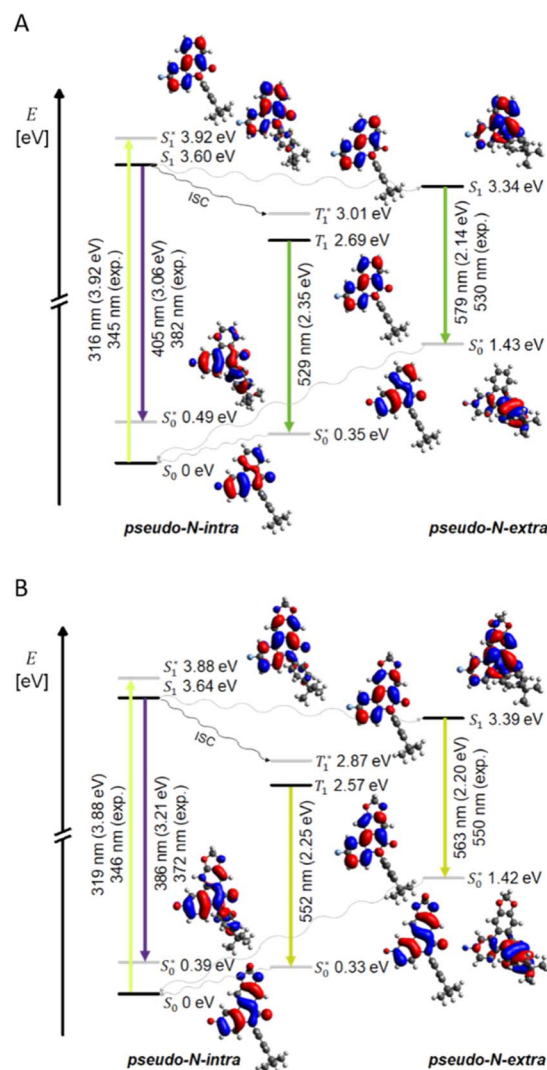

Fig. 9 Schematic Jabłoński diagrams and Kohn–Sham-FMOs of the calculated S_1 and T_1 states, including the S_0–S_1^* transition (absorption at the longest wavelength), the S_1–S_0^* transition of the *pseudo-N-intra* (LE fluorescence) and *pseudo-N-extra* (CT fluorescence), the S_1–T_1^* transition (ISC), as well as the T_1–S_0^* transition of *pseudo-N-intra* (phosphorescence) for *N*-arylphenanthridinone **4b** (A) and *N*-arylcrinasiadine **5b** (B) (Gaussian 16, B3LYP/6-31G*, PCM CH$_2$Cl$_2$, isosurface value 0.025 a.u.).

triplet quenching occurs. Furthermore, the relatively large energy gap ΔE_{ST} between T_1 and S_1 in the *pseudo-N-intra* renders an ISC unlikely. Alternatively, a conformational change to the *pseudo-N-extra* conformation might occur prior to ISC, from which a transition to the T_1 state of this geometry could take place, or an ISC to higher triplet states might occur, which could account for the low fluorescence quantum yield Φ_{em}.[35]

The localization of the LUMO on the phenanthridinone moiety in both conformers further explains the experimentally observed substituent effects on the LE to CT band ratio (Fig. 6). The weak fluorine acceptor at position R^1 stabilizes the electron density in the excited state and thus favors both bands, while electron donors would probably cause destabilization. Donors at R^2 facilitate mesomeric delocalization in the LUMO especially

in a planar geometry thus enhancing CT emission. In contrast, acceptors at R^2 withdraw electron density and destabilize the planar conformation and shift the emission ratio in favor of the LE band, which is consistent with experimental observations.

Conclusions

The consecutive sequentially palladium catalyzed three-component synthesis provides a concise approach to function-alized phenanthridinones and crinasiadines in a one-pot fashion. While *N*-aryl derivatives are obtained by this sequence, *N*-alkyl derivatives form by Suzuki arylation–lactamization followed by *N*-alkylation, also in a one-pot fashion. Particularly noteworthy is the concise synthesis of two natural products, *N*-methylcrinasiadine and *N*-phenethylcrinasiadine, whose cytotoxic effects against leukemia, lung, and colon cancer cells underscore the biological relevance of the synthetic derivatives.

Photophysical investigations reveal dual fluorescence of these compounds which can be attributed to involvement of LE (locally excited) and CT (charge transfer) states. The substitution pattern clearly affects the emission behavior, allowing fine-tuning of electronic properties to achieve desired material characteristics. Quantum chemical calculations provide initial rationalization of the origin of the LE and CT bands and suggest that the LE band emerges from the *pseudo-N-intra* conformation, while the redshifted CT band arises from the *pseudo-N-extra* conformation.

The results pave the way for the development of novel, accurately tunable phenanthridinone and crinasiadine emitters. Further studies on the syntheses of alkaloid analogues with increased emission quantum yield are currently underway.

Author contributions

The work consists of parts of the planned PhD thesis of R. K., which is supervised by T. J. J. M. Methodologic and synthetic studies, analytical characterization of the synthetic samples, photophysics (steady-state absorption and emission spectroscopy), and quantum chemical calculation by R. K., who compiled the obtained data. The conceptualization was outlined by T. J. J. M. The writing of the first draft was completed by R. K., and the review and editing was completed by R. K. and T. J. J. M. Project administration and funding acquisition by T. J. J. M. Both authors have read and agreed to the published version of the manuscript.

Conflicts of interest

There are no conflicts to declare.

Data availability

The data supporting this article have been included as part of the supplementary information (SI). Supplementary information: synthetic details, ^{1}H and ^{13}C NMR spectra, HPLC traces,

absorption and emission spectra as well as details on the (TD) DFT calculations. See DOI: https://doi.org/10.1039/d5ra06934c.

Notes and references

1 M. Feng, B. Tang, H.-X. Xu and X. Jiang, *Org. Lett.*, 2016, **18**, 4352–4355.
2 D. Liang, Z. Hu, J. Peng, J. Huang and Q. Zhu, *Chem. Commun.*, 2013, **49**, 173–175.
3 R. R. Aleti, A. A. Festa, L. G. Voskressensky and E. V. Van der Eycken, *Molecules*, 2021, **26**, 5560.
4 R. S. Theobald and K. Schofield, *Chem. Rev.*, 1950, **46**, 170–189.
5 H. Gilman and J. Eisch, *J. Am. Chem. Soc.*, 1957, **79**, 5479–5483.
6 E. C. Horning, V. L. Stromberg and H. A. Lloyd, *J. Am. Chem. Soc.*, 1952, **74**, 5153–5155.
7 C. C. Woodroofe, B. Zhong, X. Lu and R. B. Silverman, *J. Chem. Soc., Perkin Trans. 2*, 2000, 55–59.
8 K. Tanimoto, N. Nakagawa, K. Takeda, M. Kirihata and S. Tanimori, *Tetrahedron Lett.*, 2013, **54**, 3712–3714.
9 G. Wurz, O. Hofer and H. Greger, *Nat. Prod. Lett.*, 1993, **3**, 177–182.
10 H. R. Arthur, W. H. Hui and Y. L. Ng, *J. Am. Chem. Soc.*, 1959, 4007–4009.
11 H. R. Arthur, W. H. Hui and Y. L. Ng, *J. Am. Chem. Soc.*, 1959, 1840–1845.
12 T. Kametani, K. Kigasawa, M. Hiiragi and O. Kusama, *J. Heterocycl. Chem.*, 1973, **10**, 31–33.
13 X. Li, Q. Wang, L. Liu, Y. Shi, Y. Hong, W. Xu, H. Xu, J. Feng, M. Xie and Y. Li, *Pharm*, 2024, **17**, 524.
14 S. F. Martin, *The Amaryllidaceae Alkaloids*, Elsevier, San Diego, 1987.
15 G. Van Goietsenoven, A. Andolfi, B. Lallemand, A. Cimmino, D. Lamoral-Theys, T. Gras, A. Abou-Donia, J. Dubois, F. Lefranc and V. Mathieu, *J. Nat. Prod.*, 2010, **73**, 1223–1227.
16 G. Van Goietsenoven, V. Mathieu, F. Lefranc, A. Kornienko, A. Evidente and R. Kiss, *Med. Res. Rev.*, 2013, **33**, 439–455.
17 A. Evidente, A. S. Kireev, A. R. Jenkins, A. E. Romero, W. F. A. Steelant, S. Van Slambrouck and A. Kornienko, *Planta Med.*, 2009, **75**, 501–507.
18 M. Ghavre, J. Froese, M. Pour and T. Hudlicky, *Angew. Chem., Int. Ed.*, 2016, **55**, 5642–5691.
19 Z. Luo, F. Wang, J. Zhang, X. Li, M. Zhang, X. Hao, Y. Xue, Y. Li, F. D. Horgen and G. Yao, *J. Nat. Prod.*, 2012, **75**, 2113–2120.
20 M. de Fatima Pereira, C. Rochais and P. Dallemagne, *Curr. Med. Chem.:Anti-Cancer Agents*, 2015, **15**, 1080–1091.

21 J.-H. Li, L. Serdyuk, D. V. Ferraris, G. Xiao, K. L. Tays, P. W. Kletzly, W. Li, S. Lautar, J. Zhang and V. J. Kalish, *Bioorg. Med. Chem. Lett.*, 2001, **11**, 1687–1690.

22 M. Mann, S. Kumar, A. Sharma, S. S. Chauhan, N. Bhatla, S. Kumar, S. Bakhshi, R. Gupta and L. Kumar, *Oncotarget*, 2019, **10**, 4262.

23 P. Jagtap, F. G. Soriano, L. Virág, L. Liaudet, J. Mabley, É. Szabó, G. Haskó, A. Marton, C. B. Lorigados and F. Gallyas Jr, *Crit. Care Med.*, 2002, **30**, 1071–1082.

24 B. Zingarelli, S. Cuzzocrea, Z. Zsengellér, A. L. Salzman and C. Szabó, *Cardiovasc. Res.*, 1997, **36**, 205–215.

25 J. DeRuiter, B. E. Swearingen, V. Wandrekar and C. A. Mayfield, *J. Med. Chem.*, 1989, **32**, 1033–1038.

26 H. J. Crowley, B. Yaremko, W. M. Selig, D. R. Janero, C. Burghardt, A. F. Welton and M. O'Donnell, *J. Pharmacol. Exp. Ther.*, 1991, **259**, 78–85.

27 S. Pegoraro, M. Lang, T. Dreker, J. Kraus, S. Hamm, C. Meere, J. Feurle, S. Tasler, S. Prütting and Z. Kuras, *Bioorg. Med. Chem. Lett.*, 2009, **19**, 2299–2304.

28 E. Sperotto, G. P. M. van Klink, G. van Koten and J. G. de Vries, *Dalton Trans.*, 2010, **39**, 10338–10351.

29 F. Meng, X.-T. Nguyen, X. Cai, J. Duan, M. Matteucci and C. P. Hart, *Anticancer Drugs*, 2007, **18**, 435–445.

30 T. A. Grese, M. D. Adrian, D. L. Phillips, P. K. Shetler, L. L. Short, A. L. Glasebrook and H. U. Bryant, *J. Med. Chem.*, 2001, **44**, 2857–2860.

31 A. H. Parham, C. Pflumm, A. Jatsch, T. Eberle and P. Stoessel, *Organic Electroluminescent Device*, US Pat., 9337430B2, 2016.

32 R. L. d. Costa, D. A. F. da Silva, N. C. d. Lucas and S. J. Garden, *Quim. Nova*, 2016, **39**, 310–319.

33 M. Guérette, A. Najari, J. Maltais, J. R. Pouliot, S. Dufresne, M. Simoneau, S. Besner, P. Charest and M. Leclerc, *Adv. Energy Mater.*, 2016, **6**, 1502094.

34 S. K. Ganegamage, Y. Zou and M. D. Heagy, *J. Org. Chem.*, 2023, **88**, 11424–11433.

35 A. Demeter, T. Bérces and K. A. Zachariasse, *J. Phys. Chem. A*, 2001, **105**, 4611–4621.

36 D. M. D'Souza and T. J. J. Müller, *Chem. Soc. Rev.*, 2007, **36**, 1095–1108.

37 M. D. Burke and S. L. Schreiber, *Angew. Chem., Int. Ed.*, 2004, **43**, 46–58.

38 L. Brandner and T. J. J. Müller, *Front. Chem.*, 2023, **11**, 1124209.

39 G. H. Posner, *Chem. Rev.*, 1986, **86**, 831–844.

40 L. Levi and T. J. J. Müller, *Chem. Soc. Rev.*, 2016, **45**, 2825–2846.

41 T. J. J. Müller, *Science of Synthesis Series*, Georg Thieme Verlag KG, Stuttgart, 2014.

42 L. Mayer, R. Kohlbecher and T. J. J. Müller, *Chem.–Eur. J.*, 2020, **26**, 15130–15134.

43 R. Kohlbecher and T. J. J. Müller, *Chem.–Eur. J.*, 2024, **30**, e202304119.

44 H. Doucet and J. C. Hierso, *Angew. Chem., Int. Ed.*, 2007, **46**, 834–871.

45 Y. Sunesson, E. Lime, S. O. Nilsson Lill, R. E. Meadows and P.-O. Norrby, *J. Org. Chem.*, 2014, **79**, 11961–11969.

46 L. Liang, J. Li, B. Shen, Y. Zhang, J. Liu, J. Chen and D. Liu, *Org. Biomol. Chem.*, 2021, **19**, 2767–2772.

47 C. A. Moore, B. F. Ohman, M. J. Garman, M. E. Liquori, D. M. Degan, K. B. Voellinger, M. J. DePersis and E. T. Pelkey, *Arkivoc*, 2018, 50–69.

48 U. V. Mentzel, D. Tanner and J. E. Tønder, *J. Org. Chem.*, 2006, **71**, 5807–5810.

49 Y. Kuwata, M. Sonoda and S. Tanimori, *J. Heterocycl. Chem.*, 2017, **54**, 1645–1651.

50 W. H. Brown, T. Poon, *Einführung in die Organische Chemie*, Wiley-VCH, Weinheim, 2020.

51 B. E. Zaitsev, G. I. Migachev, O. V. Koval'chukova, G. V. Sheban and V. V. Matyushenko, *Chem. Heterocycl. Compd.*, 1992, **28**, 1159–1165.

52 M. J. Frisch, G. W. Trucks, H. B. Schlegel, G. E. Scuseria, M. A. Robb, J. R. Cheeseman, G. Scalmani, V. Barone, G. A. Petersson, H. Nakatsuji, X. Li, M. Caricato, A. V. Marenich, J. Bloino, B. G. Janesko, R. Gomperts, B. Mennucci, H. P. Hratchian, J. V. Ortiz, A. F. Izmaylov, J. L. Sonnenberg, D. Williams-Young, F. Ding, F. Lipparini, F. Egidi, J. Goings, B. Peng, A. Petrone, T. Henderson, D. Ranasinghe, V. G. Zakrzewski, J. Gao, N. Rega, G. Zheng, W. Liang, M. Hada, M. Ehara, K. Toyota, R. Fukuda, J. Hasegawa, M. Ishida, T. Nakajima, Y. Honda, O. Kitao, H. Nakai, T. Vreven, K. Throssell, J. J. A. Montgomery, J. E. Peralta, F. Ogliaro, M. J. Bearpark, J. J. Heyd, E. N. Brothers, K. N. Kudin, V. N. Staroverov, T. A. Keith, R. Kobayashi, J. Normand, K. Raghavachari, A. P. Rendell, J. C. Burant, S. S. Iyengar, J. Tomasi, M. Cossi, J. M. Millam, M. Klene, C. Adamo, R. Cammi, J. W. Ochterski, R. L. Martin, K. Morokuma, O. Farkas, J. B. Foresman, D. J. Fox, *Gaussian 16, Revision A.03*, Gaussian, Inc., Wallingford CT, 2016.

53 C. Lee, W. Yang and R. G. Parr, *Phys. Rev. B:Condens. Matter Mater. Phys.*, 1988, **37**, 785.

54 A. D. Becke, *J. Chem. Phys.*, 1993, **98**, 1372–1377.

55 R. Krishnan, J. S. Binkley, R. Seeger and J. A. Pople, *J. Chem. Phys.*, 1980, **72**, 650–654.

56 G. Scalmani and M. J. Frisch, *J. Chem. Phys.*, 2010, **132**, 114110.

57 I. V. Alabugin, *Stereoelectronic Effects: A Bridge between Structure and Reactivity*, John Wiley & Sons Verlag, Chichester, 2016.

58 S. Vyazovkin, *Thermochim. Acta*, 2025, **743**, 179911.

59 H. Eyring, *J. Chem. Phys.*, 1935, **3**, 107–115.

60 L. Mayer and T. J. J. Müller, *Eur. J. Org Chem.*, 2021, **2021**, 3516–3527.

61 D. Pan and D. L. Phillips, *J. Phys. Chem. A*, 1999, **103**, 4737–4743.

62 K. P. C. Vollhardt, N. E. Schore, *Organische Chemie*, John Wiley & Sons, Hannover, 2011.

63 J. Mooney and P. Kambhampati, *J. Phys. Chem. Lett.*, 2013, **4**, 3316–3318.

64 C. Würth, M. Grabolle, J. Pauli, M. Spieles and U. Resch-Genger, *Nat. Protoc.*, 2013, **8**, 1535–1550.

65 S. J. Strickler and R. A. Berg, *J. Chem. Phys.*, 1962, **37**, 814–822.

66 M. A. El-Sayed, *J. Chem. Phys.*, 1963, **38**, 2834–2838.